Constraints for non-standard interaction $\epsilon_{e\tau}V_e$ from ν_e appearance in MINOS and T2K

João A. B. Coelho, Tomas Kafka, W. Anthony Mann, Jacob Schneps, and Ozgur Altinok
Tufts University, Medford, MA 02155

Event rates for ν_e and $\overline{\nu}_e$ appearance oscillations reported by the MINOS and T2K long baseline experiments are used to set constraints on the strength of the non-standard interaction $\epsilon_{e\tau}V_e$ matter potential. The ranges allowed for the magnitude and phase of $\epsilon_{e\tau}$ are delineated for scenarios wherein *i)* other non-standard interactions for neutrinos propagating through the terrestrial crust are negligible, and *ii)* the real-valued, flavor-diagonal couplings ϵ_{ee} and $\epsilon_{\tau\tau}$ are also operative. Our analysis makes use of exact analytic forms for the ν_e amplitude $\mathcal{A}(\nu_\mu \to \nu_e)$ describing neutrino oscillation in constant-density matter in the presence of $\epsilon_{e\tau}$, ϵ_{ee} and $\epsilon_{\tau\tau}$ non-standard interactions.

PACS numbers: 14.60.Pq, 14.60.Lm, 13.15.+g

I. INTRODUCTION

Within the span of one year, multiple independent neutrino oscillation measurements by reactor and accelerator long-baseline experiments have established the neutrino θ_{13} mixing angle to be $\sim 9^\circ$ [1–5]. For neutrino oscillation experiments, the newly gained knowledge of the $\sin^2 2\theta_{13}$ mixing strength brings significant clarifications concerning sensitivity to CP-violating effects (CPV) as may ensue with either the normal hierarchy (NH) or the inverted hierarchy (IH) for the neutrino mass eigenstates.

The revelation of θ_{13} has enabled first-time determinations of "exclusion curves" for the Dirac CP phase, δ, for each mass hierarchy in experiments having sensitivity to perturbations in neutrino oscillations arising from terrestrial matter effects: The SuperKamiokande collaboration has reported χ^2 versus δ fits for NH and for IH using atmospheric neutrino data [6]; exclusion confidence level (C.L.) curves are reported by the MINOS collaboration based upon ν_e and $\overline{\nu}_e$ appearance at the experiment's 735-kilometer baseline [7]. While the exclusion levels thus far achieved are quite modest, they serve to remind that a new era of experimental scrutiny of neutrino flavor oscillations is getting underway and it remains to be seen whether conventional three-flavor mixing phenomenology will continue to be an adequate framework. Observational deviations from this framework are an exciting possibility as plausible harbingers of physics beyond the Standard Model. As a source of such deviations, the possibility that neutrinos propagating through dense matter may participate in effective, neutral-current like nonstandard interactions (NSI) has received considerable attention for more than a decade [8].

In standard three-flavor neutrino oscillation phenomenology, the Hamiltonian in flavor basis includes the Mikheyev-Smirnov-Wolfenstein (MSW) matter potential. The MSW potential accounts for coherent forward scattering of electron-flavor neutrinos from the electrons of ambient matter [9]. In an NSI scenario, the Hamiltonian carries additional matter potential terms analogous to the MSW potential which allow flavor-changing as well as flavor-conserving NSI scattering processes. There are six possible NSI amplitudes which can arise in neutrino propagation through matter. These include three real-valued, flavor-diagonal amplitudes conventionally designated as ϵ_{ee}, $\epsilon_{\mu\mu}$, and $\epsilon_{\tau\tau}$, and three flavor-changing amplitudes which may carry CP-violating phases: $\epsilon_{e\mu}$, $\epsilon_{e\tau}$, and $\epsilon_{\mu\tau}$. The phenomenology of neutrino NSI in propagation for accelerator, atmospheric, and solar neutrinos and for various beam-plus-detector(s) configurations, has received extensive treatment. Data from hadron and lepton colliders have also been utilized in NSI studies, for NSI couplings involving quarks or electrons can give rise to anomalous monojet, monophoton, and multilepton events [10]. Comprehensive citations to the published literature can be found in [8, 11–13].

The available data allow upper bounds to be set on the magnitudes of NSI couplings. According to the analysis of Ref. [14], the effective NSI parameters for terrestrial matter are $|\epsilon_{\mu\mu}| < 0.07$, $|\epsilon_{e\mu}| < 0.33$, and $|\epsilon_{\mu\tau}| < 0.33$ at 90% C.L. Additionally, on the basis of consistency with the high-energy atmospheric data, it is proposed that bounds of a few percent are appropriate for $|\epsilon_{e\mu}|$ and $|\epsilon_{\mu\tau}|$ [12, 15]. For $|\epsilon_{ee}|$, $|\epsilon_{e\tau}|$, and $|\epsilon_{\tau\tau}|$ however the bounds at 90% C.L. are much weaker; Ref. [14] finds these to be < 4.2, < 3.0, and < 21 respectively. For neutrino NSI with electrons (but not with u or d quarks), more stringent limits have been set for $\epsilon_{ee}^{eR}, \epsilon_{ee}^{eL}, \epsilon_{\tau\tau}^{eR}$, and $\epsilon_{\tau\tau}^{eL}$ based upon analysis of solar and KamLAND neutrino data [16]. With respect to NSI limits derived using monojet plus missing energy datasets of hadron collider experiments, our characterization is appropriate for the "light mediator" regime of anomalous monojet processes involving NSIs [10, 17]. Thus, at present, the $\epsilon_{e\tau}$, ϵ_{ee}, and $\epsilon_{\tau\tau}$ NSI are so poorly constrained that large matter effects, of strengths which rival or exceed that of the MSW matter potential, remain as viable phenomenological possibilities. These three couplings enter into the probabilities for ν_e appearance oscillations, and the perturbations they may introduce can be searched for by observing ν_μ and $\overline{\nu}_\mu$ beams at long baselines.

Concerning $\epsilon_{e\tau}V_e$, the current situation with the solar ^{8}B neutrino energy spectrum is worthy of note [18, 19]. The low-threshold measurements carried out thus far by Borexino, Super-Kamiokande, and the Sudbury Neutrino Observatory do not exhibit an upturn with decreasing

E_ν as predicted by standard oscillations with the MSW matter effect. However a deviation from conventional oscillations in the form of a flatter spectrum is naturally provided by an $\epsilon_{e\tau}$ coupling strength $\mathcal{O}(10^{-1})$ [17, 20].

In this work we examine manifestations of the NSI matter potential $\epsilon_{e\tau}V_e$ together with $\epsilon_{ee}V_e$ and $\epsilon_{\tau\tau}V_e$ as may occur in neutrino propagation through the constant-density terrestrial crust. We focus on ν_e and $\overline{\nu}_e$ appearance oscillations and evaluate the implications of recent signal event counts reported by the T2K (295 km) [1, 21] and MINOS (735 km) [2, 7, 22] long-baseline experiments. The sensitivity of conventional, terrestrial long-baseline experiments to the $\epsilon_{e\tau}V_e$ NSI has been explored in previous works by other researchers. In particular, experimental $\epsilon_{e\tau}V_e$ sensitivity has been examined for the 295-kilometer baseline of T2K [23], for the 735-kilometer baselines of MINOS and OPERA [24–28], for the 810-kilometer baseline of NOνA [17], and for the 1050 km baseline proposed for T2KK [12]. Several of these studies make use of constraints deduced from testing NSI scenarios using data from atmospheric neutrino experiments [15, 29, 30]. The work reported here utilizes the insights from these previous studies and examines the most recent observations of positive ν_e appearance in two accelerator beam long-baseline experiments in light of the newly delineated value range allowed to θ_{13}. Our treatment is restricted to neutral current NSI processes as may occur with neutrino propagation in matter. Complications arising from possible NSI effects in neutrino production and/or detection processes in current experiments are not considered [8].

II. OUTLINE

We proceed as follows: In Sec. III we define the matter Hamiltonian to include the NSI $\epsilon_{e\tau}$, ϵ_{ee}, and $\epsilon_{\tau\tau}$, and we assume, on the basis of bounds previously proposed [12, 14] that the $\epsilon_{\mu\mu}$, $\epsilon_{e\mu}$, and $\epsilon_{\mu\tau}$ are much smaller and can be neglected. We then present a formalism which characterizes three-flavor neutrino oscillations with NSI. Specifically, we express the ν_e appearance amplitude $\mathcal{A}(\nu_\mu \to \nu_e)$ as a sum of three terms, T_i (i=1,2,3), the absolute square of which gives the exact appearance oscillation probability for neutrinos traversing terrestrial matter of constant density. Our expressions are obtained by deriving the time evolution operator for which the three-flavor Hamiltonian including matter effects is the generator. The methodology for this approach is presented in Ref. [31]; a summary of the derivation with inclusion of the NSI considered here is given in the Appendix below. The analytic forms serve to illuminate the relative contributions arising from the various NSI and from the CP phases δ and $\delta_{e\tau}$. Their compact nature is effective in reducing input for computation, thereby increasing algorithm speeds. The analytic forms have been used to check our fits to the data which are carried out using numerical techniques.

In Sec. IV we summarize the observations of the MINOS and T2K experiments that we use in order to fit for the NSI couplings. In Sec. V we present a sequence of NSI fits to the data. We commence with a minimalist scenario, namely that $\epsilon_{e\tau}$ is the only active NSI and that its coupling is real-valued (hence neglecting its phase $\delta_{e\tau}$ degree of freedom). We then fit for the magnitude $|\epsilon_{e\tau}|$ and the sum of the CP phases $\delta+\delta_{e\tau}$. Finally we consider the realistic situation wherein complex $\epsilon_{e\tau}$ is active together with the flavor-diagonal NSI couplings ϵ_{ee}, and $\epsilon_{\tau\tau}$. For the latter we introduce a constraining relationship which is based upon the behavior of ν_μ disappearance oscillations at high energies for atmospheric neutrinos. This allows the number of variables in the fit to be limited to $|\epsilon_{e\tau}|$, ϵ_{ee}, together with the above-mentioned sum of CP phases. In Sec. VI we summarize the constraints for $|\epsilon_{e\tau}|$ which are indicated by our fits, and take note of near-term experimental developments which will enable these constraints to be improved.

III. EXACT AMPLITUDE FOR $\nu_\mu \to \nu_e$ OSCILLATIONS

A. Three-flavor oscillations with NSI matter effects

For neutrino propagation in vacuum, the Hamiltonian in the basis of three mass eigenstates ν_i (i =1, 2, 3) is

$$\hat{H}_0^{(i)} = \frac{1}{2\ell_v} \cdot \mathrm{diag}\,(0, \alpha, 1)\,, \quad \text{where} \tag{1}$$

$$\ell_v \equiv \frac{E_\nu}{\Delta m^2_{31}} \quad \text{and} \quad \alpha \equiv \frac{\Delta m^2_{21}}{\Delta m^2_{31}} \tag{2}$$

are, respectively, the vacuum oscillation length and the mass hierarchy ratio. The transformation from mass basis $\{|\nu_i\rangle\}$ to neutrino flavor basis $\{|\nu_\varphi\rangle\}$ ($\varphi = e,\ \mu,\ \tau$) is provided by the unitary mixing matrix

$$\hat{U}_{mix} \equiv \hat{R}_1(\theta_{23}) \cdot \hat{\mathbb{I}}_\delta \cdot \hat{R}_2(\theta_{13}) \cdot \hat{\mathbb{I}}_{-\delta} \cdot \hat{R}_3(\theta_{12}) \tag{3}$$

wherein the atmospheric and solar mixings are accounted for via the rotation matrices $\hat{R}_1(\theta_{23})$ and $\hat{R}_3(\theta_{12})$. The Dirac CP phase δ is included via the auxiliary matrices $\hat{\mathbb{I}}_\delta \equiv \mathrm{diag}(1, 1, e^{i\delta})$ and $\hat{\mathbb{I}}_{-\delta} = \hat{\mathbb{I}}^\dagger_\delta$. Then the vacuum Hamiltonian in flavor basis is given by the unitary transformation

$$\hat{H}_0^{(\varphi)} = \hat{U}_{mix}\hat{H}_0^{(i)}\hat{U}^\dagger_{mix}\ , \tag{4}$$

and the effective wave equation for vacuum propagation of flavor states is

$$i\frac{d}{dt}\vec{\nu}^{(\varphi)}(t) = \hat{H}_0^{(\varphi)}\vec{\nu}^{(\varphi)}(t). \tag{5}$$

To $\hat{H}_0^{(\varphi)}$ we add (in flavor basis) the MSW and NSI matter interactions:

$$\hat{H}^{(\varphi)}_{\rm matter} = V_e \begin{pmatrix} 1+\epsilon_{ee} & 0 & \epsilon_{e\tau} \\ 0 & 0 & 0 \\ \epsilon^*_{e\tau} & 0 & \epsilon_{\tau\tau} \end{pmatrix}. \tag{6}$$

Here, $V_e = \sqrt{2} G_F n_e$ is the MSW matter interaction [9] where G_F is the Fermi coupling constant and n_e is the electron density in matter. The standard MSW matter effect is modified by the presence of the real-valued, diagonal NSI interactions $\epsilon_{ee} V_e$ and $\epsilon_{\tau\tau} V_e$, and by the off-diagonal $\epsilon_{e\tau} V_e$ interaction. Since the latter amplitude may carry a CP-violating phase, $\delta_{e\tau}$, hereafter we designate the magnitude $|\epsilon_{e\tau}|$ and display the phase explicitly. It is convenient to absorb V_e into the matter potential,

$$A \equiv 2\ell_v V_e, \tag{7}$$

and to write Eq. (6) as

$$\hat{H}^{(\varphi)}_{\rm matter} = \frac{A}{2\ell_v} \begin{pmatrix} 1+\epsilon_{ee} & 0 & |\epsilon_{e\tau}|e^{i\delta_{e\tau}} \\ 0 & 0 & 0 \\ |\epsilon_{e\tau}|e^{-i\delta_{e\tau}} & 0 & \epsilon_{\tau\tau} \end{pmatrix}. \tag{8}$$

A method to solve the time evolution operator in flavor basis $\hat{U}^{(\varphi)}(t=\ell,0)$ for propagation to baseline distance ℓ in constant density matter is presented in Ref. [31], for conventional three-flavor oscillations with $\hat{H}^{(\varphi)}_{\rm matter} = {\rm diag}\,(A/2\ell_v, 0, 0)$. This same approach can be used to obtain an exact solution for the more elaborate matter interactions of Eq. (8). Following Ref. [31], the matrix elements of the evolution operator $\hat{U}^{(\varphi)}(\ell)$ corresponding to $\hat{H}^{(\varphi)}_0 + \hat{H}^{(\varphi)}_{\rm matter}$ provide the various possible three-flavor oscillation amplitudes. The ν_e appearance amplitude is given by element $\hat{U}^{(\varphi)}_{12}$ which can be broken out as a sum of three terms:

$$\mathcal{A}(\nu_\mu \to \nu_e) = T_1 + T_2 + T_3. \tag{9}$$

The component amplitudes T_i comprise an analytic foundation for our investigation of NSI constraints arising from the recent ν_e appearance observations by MINOS and T2K.

In the Sections to follow we specify the T_i and then focus upon their implications. Details concerning the derivation of the evolution operator $\hat{U}^{(\varphi)}(\ell)$ which underwrites the T_i are provided in the Appendix.

B. Specification of the T_i amplitude terms

In order to write compact expressions for the T_i, we define some notations. For the mixing angles we use $s_{ij} \equiv \sin\theta_{ij}$ and $c_{ij} \equiv \cos\theta_{ij}$; for the atmospheric oscillation phase we write

$$\Delta \equiv \frac{\Delta m^2_{31}\,\ell}{4E_\nu} = \frac{\ell}{4\ell_v}\ . \tag{10}$$

We define scaled forms α' and α'' for the hierarchy parameter :

$$\begin{aligned} \alpha' &\equiv \sin 2\theta_{12}\cdot\alpha\ , \quad \text{and} \\ \alpha'' &\equiv (1-3c^2_{12})\cdot\alpha\ . \end{aligned} \tag{11}$$

The mixing strengths involving θ_{13} are often accompanied by the factor $(1 - s^2_{12}\alpha)$, hence we define

$$\begin{aligned} \sin 2\tilde{\theta}_{13} &= (1-s^2_{12}\alpha)\cdot\sin 2\theta_{13}, \quad \text{and} \\ \cos 2\tilde{\theta}_{13} &= (1-s^2_{12}\alpha)\cdot\cos 2\theta_{13}. \end{aligned} \tag{12}$$

We need to refer to the elements of the full Hamiltonian in propagation basis as obtained after a re-phasing of its diagonal elements (see Sec. IV.B of Ref. [31]). The Hamiltonian at that stage has the form

$$\hat{H}^{(p)} = \begin{pmatrix} -Q & r & f \\ r^* & -G & b \\ f^* & b^* & +Q \end{pmatrix} \tag{13}$$

Its diagonal elements are the following real-valued functions:

$$\begin{aligned} Q &\equiv \frac{1}{4\ell_v}\left(\cos 2\tilde{\theta}_{13} - A\left[1+\epsilon_{ee} - c^2_{23}\epsilon_{\tau\tau}\right]\right), \\ G &\equiv \frac{1}{4\ell_v}\left(1 + A\left[1+\epsilon_{ee} - (2s^2_{23} - c^2_{23})\epsilon_{\tau\tau}\right] + \alpha''\right), \end{aligned} \tag{14}$$

We designate the complex-valued off-diagonal elements using lower-case letters as follows:

$$f \equiv \frac{1}{4\ell_v}\left(\sin 2\tilde{\theta}_{13} + 2c_{23}|\epsilon_{e\tau}|e^{i(\delta+\delta_{e\tau})}A\right), \tag{15}$$

$$r \equiv \frac{1}{4\ell_v}\left(c_{13}\alpha' - 2s_{23}|\epsilon_{e\tau}|e^{i\delta_{e\tau}}A\right), \tag{16}$$

$$b \equiv \frac{1}{4\ell_v}\left(-s_{13}\alpha' - s_{23}c_{23}\epsilon_{\tau\tau}e^{i\delta}A\right). \tag{17}$$

Then we have

$$T_1 = (-i)s_{23}\frac{f}{N}\cdot\sin(\bar{N}\Delta)\cdot e^{-i\delta} \tag{18}$$

where

$$\bar{N} \equiv 4\ell_v\cdot N \equiv 4\ell_v\cdot\left[|f|^2 + Q^2\right]^{\frac{1}{2}}. \tag{19}$$

The second term in Eq. (9) is

$$T_2 = (-i)c_{23}\frac{r}{\eta}\cdot\sin(\bar{\eta}\Delta)\cdot e^{i\bar{G}\Delta}, \tag{20}$$

where

$$\bar{\eta} \equiv 4\ell_v\cdot\eta \equiv 4\ell_v\cdot\left[|r|^2 + |b|^2\right]^{\frac{1}{2}}, \tag{21}$$

and

$$\bar{G} \equiv 4\ell_v\cdot G. \tag{22}$$

Of the three amplitude terms in Eq. (9), T_3 is the most intricate. If the NSIs were known to be small, e.g. $|\epsilon_{\varphi\varphi'}| \leq \alpha$, then T_3 could be neglected. However large NSIs are a distinct possibility and so T_3 is to be retained. For convenience we define two complex functions S_1 and S_2:

$$S_1 \equiv \frac{rb}{\eta^2}, \tag{23}$$

and

$$S_2 \equiv (-i)\left[\frac{|r|^2}{\eta^2}\cdot\frac{f}{N}+S_1\cdot\frac{Q}{N}\right]. \tag{24}$$

T_3 can then be expressed as

$$T_3 = -2s_{23}\cdot\{S_1\cos(\bar{\eta}\Delta)+S_2\sin(\bar{\eta}\Delta)\}\cdot\sin^2(\frac{\bar{\eta}\Delta}{2})\cdot e^{-i\delta}. \tag{25}$$

In summary, the three amplitude terms of Eq. (9) are given by Eqs. (18), (20), and (25). These can be coded as complex functions, and the $\nu_\mu \to \nu_e$ oscillation probability can be constructed as $|\mathcal{A}(\nu_\mu \to \nu_e)|^2$.

C. Appearance probability upon neglecting T_3

The ways in which NSI matter effects introduce distortions to conventional oscillations can be discerned in part by examining an approximate form for the ν_e appearance probability $\mathcal{P}(\nu_\mu \to \nu_e)$. Under the assumption that all $\epsilon_{\varphi\varphi'}$ are relatively small, we may neglect T_3 and write

$$\begin{aligned}|\mathcal{A}(\nu_\mu \to \nu_e)|^2 \simeq |T_1+T_2|^2 &= s_{23}^2\cdot|f|^2\cdot\frac{\sin^2(\bar{N}\Delta)}{N^2}\\ &+\sin 2\theta_{23}\cdot\frac{\sin(\bar{N}\Delta)}{\bar{N}}\cdot\frac{\sin(\bar{\eta}\Delta)}{\bar{\eta}}\cdot\\ &\Big\{c_{13}\sin 2\tilde{\theta}_{13}\cdot\alpha'\cdot\cos(\bar{G}\Delta+\delta)\\ &-2s_{23}\sin 2\tilde{\theta}_{13}\cdot|\epsilon_{e\tau}|A\cdot\cos(\bar{G}\Delta+\delta+\delta_m)\\ &+2c_{23}c_{13}\cdot\alpha'\cdot|\epsilon_{e\tau}|A\cdot\cos(\bar{G}\Delta-\delta_m)\\ &-2\sin 2\theta_{23}\cdot(|\epsilon_{e\tau}|A)^2\cdot\cos(\bar{G}\Delta)\Big\}\\ &+c_{23}^2\cdot\frac{|r|^2}{\eta^2}\cdot\sin^2(\bar{\eta}\Delta).\end{aligned} \tag{26}$$

In the last term, the ratio $\frac{|r|^2}{\eta^2}$ reduces to c_{13}^2 in the limit that the NSI couplings go to zero. More generally, the oscillation probability of Eq. (26) reduces to the three leading terms of the exact formula of Ref. [31] in the limit that the NSI interactions are turned off. As discussed in Ref. [31], these same three terms are related to the well-known perturbative formula of Cervera *et al.* (Ref. [35]; see also [36], [37]). One manifestation of a sizable $|\epsilon_{e\tau}|$ occurs within the factor $|f|^2$ of the first term of Eq. (26). Referring to Eq. (15), one sees that the term containing $|\epsilon_{e\tau}|e^{i(\delta+\delta_{e\tau})}A$ causes the effective mixing strength to deviate from $\sin 2\tilde{\theta}_{13}$, giving a dependence upon E_ν. Amplitude expressions which lead to $\mathcal{P}(\nu_\mu \to \nu_e)$ of accuracy comparable to Eq. (26) have been discussed in previous works [11, 27].

IV. ν_e APPEARANCE IN T2K AND MINOS

The occurrence of electron-shower dominated events with rates as predicted for $\nu_\mu \to \nu_e$ oscillations, has recently been reaffirmed by the T2K and MINOS long-baseline experiments. In T2K, data exposures to the experiment's low-energy, off-axis (2.5°) ν_μ beam totaling 2.56×10^{20} protons-on-target (PoT) have been analyzed. Among events having reconstructed energies less than 1250 MeV, 10 ν_e charged-current event candidates are observed, to be compared to 2.47 background events predicted for null oscillations [21]. The ten candidate signal events include six ν_e events reported previously by T2K as evidence for a relatively large θ_{13} mixing angle [1].

The recent MINOS results are based on exposures to the NuMI low-energy beam of 10.6×10^{20} PoT in neutrino-focusing mode and 3.3×10^{20} PoT in antineutrino-focusing mode. It is reported that, from data runs with ν_μ-focusing, 152 candidate ν_e events are observed while 128.6 events are expected for null oscillations. (For NH with $\sin^2 2\theta_{13}=0.10$ and $\delta_{CP}=0$, 161.1 events are expected.) For running with $\overline{\nu}_\mu$-focusing (reversed horn-current running), 20 ($\overline{\nu}_e+\nu_e$) candidate events are observed, while 17.5 events are expected for null oscillations. (For NH with $\sin^2 2\theta_{13}=0.10$ and $\delta_{CP}=0$, 21.2 events are expected.) [22].

For the purpose of fitting to NSI scenarios, we treat both experiments as counting experiments in which a signal has been measured over and above an estimated background. Errors are assigned according to sample statistics plus allowance for systematic errors associated with background estimation and signal detection. For MINOS we allot a conservative systematic error estimate of 6% [2]; for T2K we allot 15% [1, 21]. For the 295-km baseline of T2K and for the 735-km baseline of MINOS as well, neutrino propagation is confined to the Earth's crust, for which a density of $\rho=2.72$ g/cm^3 is assumed. In fitting of three-flavor neutrino oscillations with matter effects, we use $V_e=1.1\times10^{-13}$ eV $=(1/1900)$ km^{-1} [32].

V. ALLOWED REGIONS FOR $\epsilon_{e\tau}$

We proceed with fitting of three-flavor neutrino oscillations including NSI to the T2K and MINOS ν_e appearance data. A log-likelihood fit of three terms is used to compare the observed versus expected signal rates for ν_e appearance in T2K, and for ν_e appearance and $\overline{\nu}_e$ appearance in MINOS. As previously noted, we neglect the NSI $\epsilon_{\mu\mu}$, $\epsilon_{e\mu}$, and $\epsilon_{\mu\tau}$ on the basis of the existing upper bounds, and focus on the possible role for $\epsilon_{e\tau}$ which may be operative in conjunction with ϵ_{ee} and $\epsilon_{\tau\tau}$. Even with restriction to the latter three NSI, the number of degrees of freedom available to an oscillation scenario remains rather daunting, for the CP phases δ and $\delta_{e\tau}$ are present together with the three coupling strengths, and the two possibilities for the mass hierarchy must be considered. Additionally the fits require values to be specified for the atmospheric $\Delta m^2_{31}$and solar Δm^2_{21} mass-squared differences and for the mixing angles θ_{23}, θ_{13}, and θ_{12}. For these we use the world-average values and 1 σ error ranges obtained for the normal hierarchy

by Ref. [38].

In the fits, the probabilities are computed by constructing a numeric Hamiltonian in flavor basis, solving for its eigensystem, and using it to propagate the neutrino amplitudes. The oscillation probabilities are then assembled and multiplied by "event densities" constructed so as to yield the differential event rates predicted for null oscillations. For each experiment, integration of the oscillation-weighted event density over the neutrino energy range probed provides the number of events predicted in the presence of oscillations. The prediction is then compared to the observed number of events using the log-likelihood distribution given below:

$$\chi^2 = -2\sum_{i=1}^{3} \ln \mathcal{L}(N_p^i \,|\, N_{obs}^i, \sigma_p^i) + \chi^2_{\rm penalty} \ , \qquad (27)$$

where

$$-\ln \mathcal{L}(N_p \,|\, N_{obs}, \sigma_p) =$$
$$\min_{\xi} \left\{ N_p(1+\xi) - N_{obs} + N_{obs} \ln \left[\frac{N_{obs}}{N_p(1+\xi)} \right] + \frac{(\xi N_p)^2}{2\,\sigma_p^2} \right\}$$

and

$$\chi^2_{\rm penalty} = \frac{(s_{13} - \bar{s}_{13})^2}{\delta \bar{s}_{13}{}^2} + \frac{(s_{23} - \bar{s}_{23})^2}{\delta \bar{s}_{23}{}^2}. \qquad (28)$$

In the above expressions N_p^i and N_{obs}^i are the predicted and observed number of events respectively, for experimental measurements $i = 1, 2, 3$. The systematic uncertainty of N_p^i is denoted by σ_p^i and is taken into account by minimizing the nuisance parameter ξ representing a fractional shift in N_p^i. Current best-fit values for $\sin^2\theta_{13}$ and $\sin^2\theta_{23}$ are assigned to $\bar{s}_{13}$ and $\bar{s}_{23}$, and their uncertainties are given by $\delta\bar{s}_{13}$ and $\delta\bar{s}_{23}$. For all fits reported below, marginalization is carried out for $\sin^2\theta_{23}$ and $\sin^2\theta_{13}$ [38].

A. Real-valued $\epsilon_{e\tau}$ as sole operative NSI

As a first step, we consider a minimalist scenario in which $\epsilon_{e\tau}$ is the only operative NSI which we restrict to be real-valued, allowing it to be positive or negative but otherwise ignoring its phase degree of freedom. We carry out two sets of fits with NH and IH treated separately in each set. For the first set the value zero is assigned to the Dirac CP phase δ, while for the second set the range 0 to 2π of δ is marginalized over in the fits. In both sets the data is fitted to $\nu_\mu(\overline{\nu}_\mu) \to \nu_e(\overline{\nu}_e)$ oscillations with $\epsilon_{e\tau} V_e$ included together with the conventional MSW matter effect. The distributions of $\Delta\chi^2 \equiv \chi^2 - \chi^2$(best-fit) from the two sets of fits are shown in Figure 1. The distributions serve as exclusion curves, with values of $\epsilon_{e\tau}$ having $\Delta\chi^2$ which exceed 1.0 (2.71) being excluded at 68%(90%)

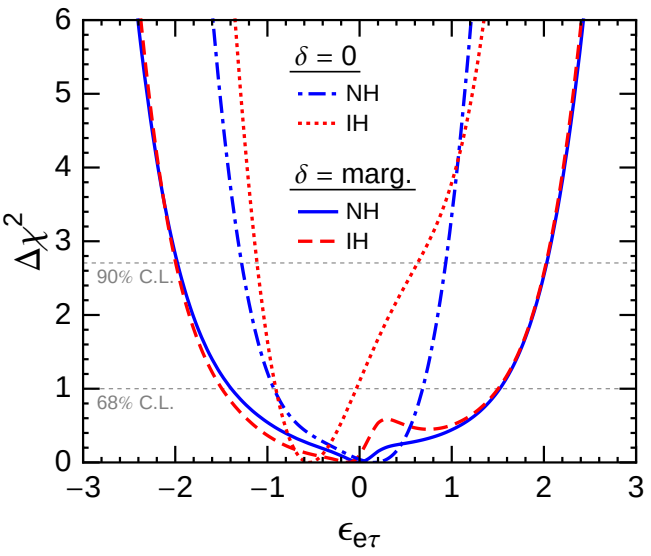

FIG. 1. Distributions of $\Delta\chi^2$ from fitting ν_e and $\overline{\nu}_e$ appearance rates reported by MINOS and T2K to $\nu_\mu(\overline{\nu}_\mu) \to \nu_e(\overline{\nu}_e)$ oscillations with the $\epsilon_{e\tau}$ NSI restricted to real values. All fits are marginalized over the allowed ranges for the θ_{23} and θ_{13} mixing angles. For the fits of the dot-dash line (NH) and dotted line (IH) distributions, the Dirac CP phase, δ, is set to zero. With δ marginalized in the fitting, the bounds on real-valued $\epsilon_{e\tau}$ become less stringent as shown by the solid line (NH) and dashed line (IH) distributions.

C.L. The first set of fits with the values of both CP phases assigned to zero, yield the dot-dash line ($\Delta m^2_{31} > 0$) and dotted line ($\Delta m^2_{31} < 0$) distributions. The distributions indicate $|\epsilon_{e\tau}| \leq 1.3$ at 90% C.L. for either mass hierarchy. For the same scenario but with solar scale mixing also neglected ($\alpha \to 0$), more stringent bounds have been obtained by fitting to atmospheric plus K2K neutrino oscillation data [29]. However the bounds become distinctly more relaxed when the Dirac CP phase δ is accounted for via marginalization, as shown by solid line (NH) and dashed line (IH) distributions from the second set of fits. The latter exclusion curves are nearly identical and so the hierarchies are not distinguished. At 90% C.L. our fits to real-valued $\epsilon_{e\tau}$ with δ marginalization yield the constraint

$$-2.0 < \epsilon_{e\tau} < 2.0 \ , \qquad (29)$$

for either mass hierarchy.

B. $|\epsilon_{e\tau}|e^{i\delta_{e\tau}}$ as sole operative NSI

For our second scenario we continue to treat $\epsilon_{e\tau}$ as the sole operative NSI, however we now treat it as a complex amplitude by including both its magnitude $|\epsilon_{e\tau}|$ and its CP phase $\delta_{e\tau}$ in the fit. Additonally we allow the Dirac CP phase to be operative. At T2K and MINOS baselines the contribution from solar scale oscillations can be

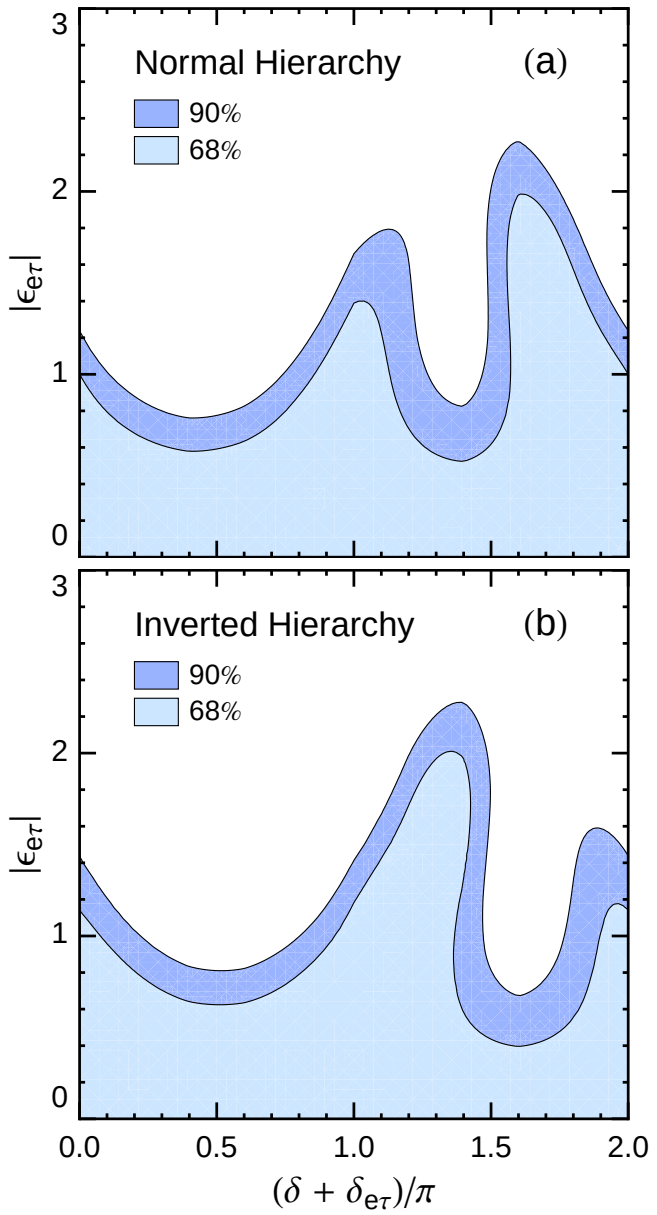

FIG. 2. Allowed-region contours of $\Delta\chi^2$ from fitting to three-flavor neutrino oscillations with $|\epsilon_{e\tau}|e^{i\delta_{e\tau}}V_e$ as the only operative NSI matter potential. The regions allowed to $|\epsilon_{e\tau}|$ and $(\delta + \delta_{e\tau})$ are shown separately for the NH (Fig. 2a) and IH (Fig. 2b) neutrino mass hierarchies. In each Figure, values within the shaded region bounded by the upper (lower) border are allowed by the fit at 90% (68%) C.L.

regarded as a perturbation, and a simplification arises in the limit of no solar scale which can be harnessed to good effect. As has been known for some time, the phases δ and $\delta_{e\tau}$, in the limit $\alpha \to 0$, only appear in the ν_e appearance probability as the sum $\delta + \delta_{e\tau}$ [12, 39]. The verity of this assertion can be discerned in part by considering the oscillation probability of Eq. (26). In Eq. (26), the first term contains $(\delta + \delta_{e\tau})$ as the phase of the amplitude, f, and the third term contains the same phase combination within an oscillatory cosine; otherwise the second and fourth terms vanish in the limit $\alpha \to 0$, and the fifth and sixth terms are devoid of phases.

With careful consideration of the T_3 amplitude of Eq. (25) and of the terms of $\mathcal{P}(\nu_\mu \to \nu_e)$ in which it enters ($T_3 T^*_{1,2} + T^*_3 T_{1,2}$ and $|T_3|^2$), the fact that the CP phases only appear in the $\alpha \to 0$ limit as the sum $(\delta + \delta_{e\tau})$ can be seen to hold exactly for ν_e appearance in constant-density matter.

Since the null solar-scale limit identifies $(\delta + \delta_{e\tau})$ to be the predominant source of phase in $\mathcal{P}(\nu_\mu \to \nu_e)$, we express all phases within $\mathcal{P}(\nu_\mu \to \nu_e)$ in terms of the sum and the difference $\delta \pm \delta_{e\tau}$. We then use the sum-of-phases together with $|\epsilon_{e\tau}|$ as fit parameters, and marginalize over the difference-of-phases. As was done for the fit of Fig. 1, we also marginalize over the θ_{23} and θ_{13} mixing angles. The χ^2 fit identifies the regions allowed to the values $|\epsilon_{e\tau}|$ and $(\delta + \delta_{e\tau})$ as shown in Fig. 2. Figure 2a shows the result of fitting to the NH; the result for IH is shown in Fig. 2b. Within each plot, the parameter regions allowed by the fit at 68% and 90% C.L. are the shaded areas bounded by the lower and upper borders respectively.

For either hierarchy, there are sizable intervals for the sum-of-phases wherein $|\epsilon_{e\tau}|$ is constrained at 90% C.L. to values distinctly smaller than the limit obtained with our fit result of Eq. (29). The improved constraints for $|\epsilon_{e\tau}|$ in Fig. 2 are made possible by allowing $(\delta + \delta_{e\tau})$ to be a fit parameter; the marginalization of the phase δ for the fit of Fig. 1 effectively selects phases from regions of large excursion in $|\epsilon_{e\tau}|$ as appear in Figs. 2a,b.

C. $\epsilon_{e\tau}$, ϵ_{ee}, $\epsilon_{\tau\tau}$ with atmospheric constraints

Given that current limits for ϵ_{ee} and $\epsilon_{\tau\tau}$ are even less stringent than those for $\epsilon_{e\tau}$, full coverage of the possibilities requires that all three of these NSI be treated as operative. Then $|\epsilon_{e\tau}|$, ϵ_{ee}, $\epsilon_{\tau\tau}$, and $(\delta + \delta_{e\tau})$ will have significant roles in the fit; on the other hand our data only consists of three "bins" of signal rates. We are thus motivated to utilize two observations gleaned from analysis of this same NSI scenario using the atmospheric neutrino data.

The first observation is that the allowed region of NSI couplings is well-characterized by an analytic expression [29, 30]:

$$\epsilon_{\tau\tau} \simeq |\epsilon_{e\tau}|^2/(1 + \epsilon_{ee}). \tag{30}$$

Relation (30) is implied by the requirement that oscillations with our three NSI couplings be consistent with the high-energy atmospheric neutrino data [12]. For our final fit we assume relation (30) to express an equality; with this assumption $\epsilon_{\tau\tau}$ can be expressed in terms of $|\epsilon_{e\tau}|$ and ϵ_{ee}, thereby reducing the number of NSI fit parameters. Of course, we could as well use Eq. (30) to eliminate ϵ_{ee} instead of $\epsilon_{\tau\tau}$; both approaches have been pursued in the literature [12, 27].

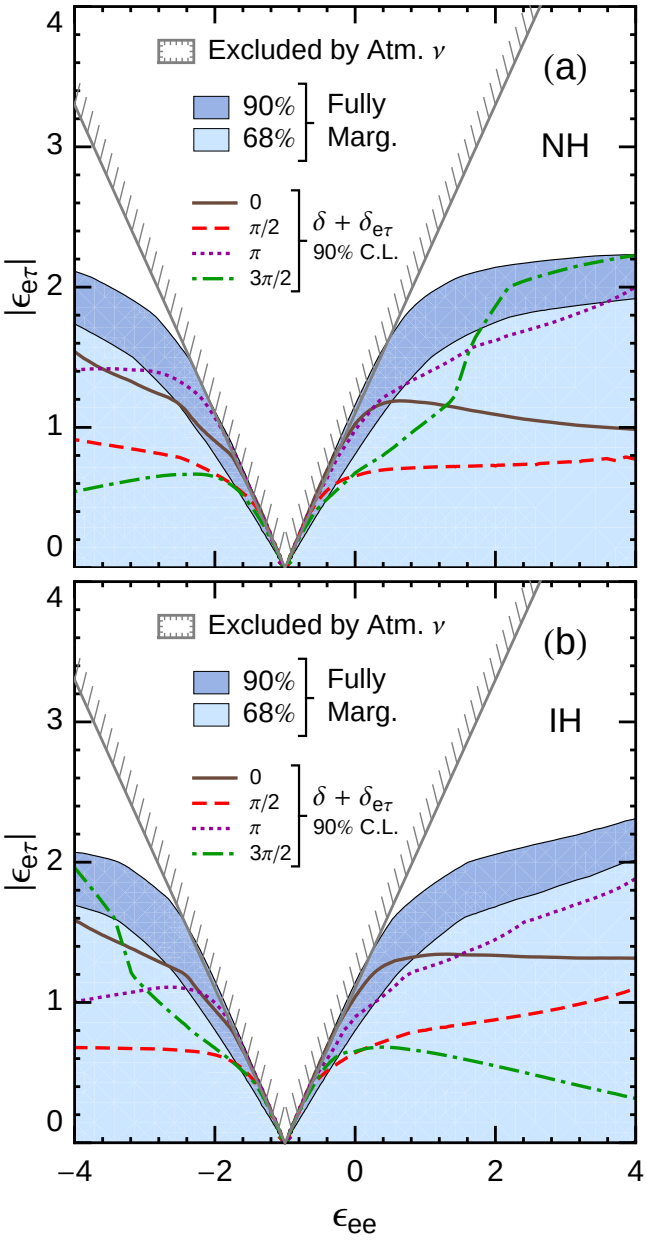

FIG. 3. Allowed and excluded regions in the plane of $|\epsilon_{e\tau}|$ versus ϵ_{ee} for (a) NH and for (b) IH. Shaded areas denote parameter regions allowed upon fitting to T2K and MINOS data, with marginalization over δ and $\delta_{e\tau}$, as well as over θ_{23} and θ_{13}. The V-shaped interior region (see Eq. (31)) is excluded on the basis of atmospheric neutrino and K2K data [12]. The fit sensitivity to CP phases is indicated using separate fits in which the value of $\delta+\delta_{e\tau}$ is fixed to, e.g. 0, $\frac{\pi}{2}$, π, or $\frac{3\pi}{2}$. These give rise to upper boundaries at 90% C.L. for $|\epsilon_{e\tau}|$ as shown by the four curves in each plot (solid, dashed, dotted, and dot-dashed respectively).

The second observation is an approximate bound deduced from atmospheric neutrino data [12, 30]:

$$|\epsilon_{e\tau}| \leq 1.1 \times |1 + \epsilon_{ee}|. \qquad (31)$$

In the following we use relation (31) in conjunction with exclusion curves obtained from fitting to establish constraints for $|\epsilon_{e\tau}|$. For this purpose relation (31) is very useful, for it eliminates a narrow region of otherwise viable solutions for which $(1 + \epsilon_{ee}) \sim 0$ and hence $\epsilon_{\tau\tau}$, via Eq. (30), can be exceedingly large.

For our final set of χ^2 fits, we use $|\epsilon_{e\tau}|$ and ϵ_{ee} as fit parameters. Figure 3 displays our fit results as allowed regions in the plane of $|\epsilon_{e\tau}|$ versus ϵ_{ee} with the distinction made between the neutrino mass hierarchies, NH in Fig. 3a versus IH in Fig. 3b. The straight-line borders of the wedge-shaped region excluded by the atmospheric ν constraint as encoded by Eq. (31), are superposed on each plot of Fig. 3.

Four separate fits have been carried out in which the sum of phases $(\delta + \delta_{e\tau})$ is fixed to a specific value in each fit, namely 0, $\frac{\pi}{2}$, π, and $\frac{3\pi}{2}$, while the difference in CP phases $(\delta - \delta_{e\tau})$ is marginalized over. The outcomes are summarized by the four curves (solid-line, dashed, dotted, and dot-dash curves respectively) which appear within the shaded areas of each plot. The curves represent the boundaries which separate the regions of allowed $(|\epsilon_{e\tau}|,\ \epsilon_{ee})$ values (areas below the curves) from those which are excluded at 90% C.L. These results clearly suggest that limiting or measuring $|\epsilon_{e\tau}|$ at strengths below the MSW matter effect is a goal for the longer term. At the baselines considered here, even hierarchy discrimination in conjunction with a precision δ measurement does not assure that very restrictive limits are achievable.

Our most realistic fits however are ones for which both of the CP phases are included in the marginalization. The outcomes of these latter fits define the parameter regions allowed to $|\epsilon_{e\tau}|$ and ϵ_{ee} at 68% and 90% C.L. as depicted by the shaded areas in Figs. 3a,b. Thus the net effect of the recent T2K and MINOS data is to exclude those regions of relatively high $|\epsilon_{e\tau}|$which lie above the shaded allowed regions and are exterior to the region previously disfavored by the atmospheric neutrino data.

VI. DISCUSSION

Previous investigations of NSI matter effects in neutrino oscillations were hindered by lack of a measured value for the θ_{13} mixing angle. The present work has availed itself of the recent delineation of θ_{13}; it is the first study to use ν_e and $\overline{\nu}_e$ appearance measurements from accelerator long-baseline experiments, in conjunction with atmospheric-neutrino measurements, to obtain constraints for the complex $\epsilon_{e\tau}$ NSI coupling. The constraints are expressed by the allowed regions in Figures 2 and 3. The limiting values for $|\epsilon_{e\tau}|$ vary according to the sum of the CP-violating phases $\delta + \delta_{e\tau}$ and according to the choice of neutrino mass hierarchy. At 90% C.L. the maximum value allowed to $|\epsilon_{e\tau}|$ varies from 0.7 to 2.3, as shown by the minima and maxima in the allowed regions versus $\delta+\delta_{e\tau}$ for each mass hierarchy. These values represent an improvement upon the limit $|\epsilon_{e\tau}| < 3.0$ pre-

viously inferred from world data [14]. Nevertheless, the allowed range for $|\epsilon_{e\tau}|$ permitted by our analysis is still relatively large, with the strength of the NSI potential exceeding that of the conventional MSW matter effect remaining as a viable possibility. Our fit results of Fig. 3 show that, with the flavor-diagonal NSI $\epsilon_{\tau\tau}$ expressed in terms of $|\epsilon_{e\tau}|$ and ϵ_{ee} using the atmospheric relation (30), the ν_e appearance data does not provide any upper limits to the magnitude of the ϵ_{ee} NSI. A ν_e appearance measurement to constrain ϵ_{ee} will likely require significantly more data, obtained with detectors located at two different baselines such as in the 295 km and 1050 km baselines of the T2KK proposal [12].

In the near term, the T2K experiment is pursuing a precision measurement of $\mathcal{P}(\nu_\mu \to \nu_e)$ with ν_μ exposures continuing at higher beam power. A ν_e appearance sample with sevenfold more events is projected for 2015 [21]. For the MINOS experiment on the other hand, running with the NuMI neutrino beam in its low-energy configuration has completed. A new round of data taking with the MINOS detectors will commence in 2013 with the NuMI beam operating in medium-energy mode, for the MINOS+ experiment. With medium-energy running, neutral-current interactions yielding shower-like final states will occur at higher rates than was the case in MINOS exposures and so ν_e appearance measurements in MINOS+ may not be feasible. Medium-energy running of the NuMI beam however is optimal for ν_e appearance measurements using NOνA. The 810-km long baseline of NOνA is off-axis with respect to the NuMI beam; it receives a narrow-band neutrino flux for which backgrounds originating from high energy neutral-current reactions are mostly suppressed. It is the NOνA experiment whose observations of $\nu_e/\overline{\nu}_e$ appearance rates and spectra, when taken together with new T2K measurements, hold promise for significant gains in delimiting NSI matter effects for neutrinos in propagation [17]. The discovery reach for NSI of the projected T2K and NOνA exposures, when combined with measurements from the reactor experiments, has been examined in Ref. [40]. A point often made is that a degree of redundancy among the international suite of neutrino long-baseline accelerator and reactor experiments is useful for delineating the standard three-flavor oscillation framework. With NSI matter effects for neutrinos in propagation included for consideration, multiple measurements conducted at different baselines will be essential to affirming or ruling out the $\epsilon_{e\tau}$ non-standard interaction.

ACKNOWLEDGMENTS

This work was supported by the United States Department of Energy under grant DE-FG02-92ER40702.

APPENDIX: DERIVATION OF $\mathcal{A}(\nu_\mu \to \nu_e)$ INCLUDING $\epsilon_{e\tau}$, ϵ_{ee}, AND $\epsilon_{\tau\tau}$ NSI

Our derivation of the exact $\mathcal{A}(\nu_\mu \to \nu_e)$ for the matter Hamiltonian of Eq. (8) for neutrinos propagating through a constant-density medium, proceeds as described in Sec. IV of Ref. [31]. In brief, the conventional three-flavor Hamiltonian in flavor basis $\hat{H}^{(\varphi)}$ is transformed to the propagation basis $\hat{H}^{(p)}$. Upon re-phasing of the diagonal elements of $\hat{H}^{(p)}$ (with minor differences from the description in Ref. [31]), one arrives at the Hamiltonian of Eq. (13). We separate $\hat{H}^{(p)}$ into an "unperturbed" part, $\hat{H}_0^{(p)}$, plus an interaction potential, $\hat{\mathbb{V}}$:

$$\hat{H}_0^{(p)} + \hat{\mathbb{V}} = \begin{pmatrix} -Q & 0 & f \\ 0 & -G & 0 \\ f^* & 0 & +Q \end{pmatrix} + \begin{pmatrix} 0 & r & 0 \\ r^* & 0 & b \\ 0 & b^* & 0 \end{pmatrix}. \quad (32)$$

We then define an Interaction Picture:

$$\vec{\nu}^{(I)}(t) = e^{i\hat{H}_0^{(p)}t}\vec{\nu}^{(p)}(t),\ \vec{\nu}^{(p)}(t) = e^{-i\hat{H}_0^{(p)}t}\vec{\nu}^{(I)}(t)\ , \quad (33)$$

so that

$$i\frac{d}{dt}\vec{\nu}^{(I)}(t) = \hat{V}_I \cdot \vec{\nu}^{(I)}(t) \quad (34)$$

where

$$\hat{V}_I(t) = e^{i\hat{H}_0^{(p)}t} \cdot \hat{\mathbb{V}} \cdot e^{-i\hat{H}_0^{(p)}t}. \quad (35)$$

Our approach is to solve for the time evolution operator in the Interaction Picture $\hat{U}_I(t = \ell,\, t = 0)$:

$$\vec{\nu}^{(I)}(t) = \hat{U}_I(t,0) \cdot \vec{\nu}^{(I)}(0). \quad (36)$$

Substitution of Eq. (36) into Eq. (34) yields the wave equation which governs $\hat{U}_I(t,0)$:

$$i\frac{d}{dt}\hat{U}_I(t,0) = \hat{V}_I(t)\hat{U}_I(t,0). \quad (37)$$

To obtain $\hat{V}_I(t)$ we require the matrix representation (in propagation basis) of the unitary operator forms $\exp(\pm i\hat{H}_0^{(p)}t)$. From $\hat{H}_0^{(p)}$ we extract the reduced matrix

$$\hat{H}_{0,R}^{(p)} = \begin{pmatrix} -Q & f_0 + if_1 \\ f_0 - if_1 & +Q \end{pmatrix}, \quad (38)$$

where f_0 and f_1 designate the real and imaginary parts of the element $(\hat{H}_0^{(p)})_{13} \equiv f$. The reduced matrix can be decomposed using Pauli matrices,

$$\begin{aligned} \hat{H}_{0,R}^{(p)} &= f_0\hat{\sigma}_x - f_1\hat{\sigma}_y - Q\hat{\sigma}_z \\ &= \vec{N} \cdot \vec{\sigma},\ \text{ where }\ \vec{N} = (f_0, -f_1, -Q). \end{aligned} \quad (39)$$

We have $|\vec{N}| = N = \sqrt{f_0^2 + f_1^2 + Q^2}$. Its unit vector $\hat{n}$ defines the axis of rotation in the reduced (spinor) space,

$$\hat{n} = (n_x,\ n_y,\ n_z) = \frac{1}{(|f|^2 + Q^2)^{\frac{1}{2}}}\,(f_0, -f_1, -Q)\,. \quad (40)$$

Designating the angle of rotation with

$$\phi \equiv N\ell, \tag{41}$$

we use the spinor identity

$$e^{i\vec{\sigma}\cdot\hat{n}\phi} = \begin{pmatrix} \cos\phi + in_z\sin\phi & (in_x + n_y)\cdot\sin\phi \\ (in_x - n_y)\cdot\sin\phi & \cos\phi - in_z\sin\phi \end{pmatrix} \tag{42}$$

and furthermore define

$$\begin{aligned} &\gamma \equiv \cos\phi + in_z\sin\phi, \\ &\beta \equiv \beta_x + i\beta_y,\ \beta_x \equiv n_x\sin\phi,\ \beta_y \equiv n_y\sin\phi. \end{aligned} \tag{43}$$

Then $i\beta = i\beta_x - \beta_y$ and $i\beta^* = i\beta_x + \beta_y$, and we have

$$e^{i\hat{H}^{(p)}_{0,R}\ell} = e^{i\vec{\sigma}\cdot\hat{n}(N\ell)} = \begin{pmatrix} \gamma & i\beta^* \\ i\beta & \gamma^* \end{pmatrix}. \tag{44}$$

Thus in the propagation basis we may write

$$e^{i\hat{H}^{(p)}_{0}\ell} = \begin{pmatrix} \gamma & 0 & i\beta^* \\ 0 & e^{-iG\ell} & 0 \\ i\beta & 0 & \gamma^* \end{pmatrix}. \tag{45}$$

To move the formalism to the Interaction Picture, we evaluate

$$\begin{aligned} \hat{V}_I(\ell) &= e^{i\hat{H}^{(p)}_0\ell}\cdot\hat{\mathbb{V}}\cdot e^{-i\hat{H}^{(p)}_0\ell} \\ &= \begin{pmatrix} 0 & u & 0 \\ u^* & 0 & v \\ 0 & v^* & 0 \end{pmatrix}, \end{aligned} \tag{46}$$

where the complex elements of $\hat{V}_I(\ell)$ are

$$u \equiv (\gamma r + i\beta^* B)e^{iG\ell},\ \ v \equiv (\gamma B - i\beta^* r^*)e^{-iG\ell}. \tag{47}$$

Now

$$\left(\hat{V}_I(\ell)\right)^2 = \begin{pmatrix} |u|^2 & 0 & uv \\ 0 & |u|^2 + |v|^2 & 0 \\ (uv)^* & 0 & |v|^2 \end{pmatrix}. \tag{48}$$

The real-valued expression $(|u|^2+|v|^2)$ recurs upon taking higher integer powers of $\hat{V}_I(\ell)$. It is readily reduced to $(|r|^2 + |b|^2)$, previously designated as η^2 in Eq. (21):

$$\eta^2 = |u|^2 + |v|^2 = |r|^2 + |b|^2. \tag{49}$$

The exponentiation of $\hat{V}_I(\ell)$ into $e^{-i\hat{V}_I\ell}$ proceeds as in Ref. [31]. We obtain

$$e^{-i\hat{V}_I\ell} = \hat{\mathbb{I}} - \left(\frac{\hat{V}_I}{\eta}\right)^2(1 - \cos(\eta\ell)) - i\frac{\hat{V}_I}{\eta}\sin(\eta\ell). \tag{50}$$

We define

$$\theta \equiv \eta\ell,\ \ \bar{u} \equiv \frac{u}{\eta},\ \ \bar{v} \equiv \frac{v}{\eta}, \tag{51}$$

and write the diagonal elements of Eq. (50) as

$$D_u \equiv 1 - 2|\bar{u}|^2\cdot\sin^2\frac{\theta}{2},\ d \equiv \cos\theta,\ D_v \equiv 1 - 2|\bar{v}|^2\cdot\sin^2\frac{\theta}{2}. \tag{52}$$

For the off-diagonal elements we define

$$w \equiv \bar{u}\sin\theta,\ \ p \equiv -2\bar{u}\bar{v}\sin^2\frac{\theta}{2},\ \ k \equiv \bar{v}\sin\theta\ . \tag{53}$$

Then the evolution operator in the Interaction Picture is

$$\hat{U}_I(\ell,0) = e^{-i\hat{V}_I\ell} = \begin{pmatrix} D_u & -iw & p \\ -iw^* & d & -ik \\ p^* & -ik^* & D_v \end{pmatrix} \tag{54}$$

and, in the propagation basis, it becomes

$$\begin{aligned} &\hat{U}^{(p)}(\ell,0) = e^{-i\hat{H}^{(p)}_0\ell}\cdot\hat{U}_I(\ell,0) \\ &= \begin{pmatrix} \gamma^*D_u - i\beta^*p^* & \gamma^*(-iw) - \beta^*k^* & \gamma^*p - i\beta^*D_v \\ -iw^*e^{iG\ell} & de^{iG\ell} & (-ik)e^{iG\ell} \\ \gamma p^* - i\beta D_u & \gamma(-ik^*) - \beta w & \gamma D_v - i\beta p \end{pmatrix}. \end{aligned} \tag{55}$$

Finally, returning to flavor basis

$$\hat{U}^{(\varphi)}(\ell,0) = (\hat{R}_1\hat{\mathbb{I}}_\delta)\cdot\hat{U}^{(p)}(\ell,0)\cdot(\hat{\mathbb{I}}_{-\delta}\hat{R}_1^T) \tag{56}$$

we obtain

$$\begin{aligned} &(\hat{U}^{(\varphi)})_{12} = \mathcal{A}(\nu_\mu\to\nu_e) = \\ &c_{23}U^{(p)}_{12} + s_{23}U^{(p)}_{13}e^{-i\delta} = \\ &(-i)c_{23}(\gamma^*w - i\beta^*k^*) + s_{23}\gamma^*pe^{-i\delta} - is_{23}\beta^*D_ve^{-i\delta}. \end{aligned} \tag{57}$$

We insert expressions (52) and (53) for the elements of k, p, and D_v into the last line of Eq. (57) and re-arrange the order of the terms to obtain

$$\begin{aligned} \mathcal{A}(\nu_\mu\to\nu_e) = &(-i)s_{23}\beta^*e^{-i\delta} \\ &+ (-i)c_{23}\left[\gamma^*\bar{u} - i\beta^*\bar{v}^*\right]\sin\theta \\ &+ 2s_{23}\left[i\beta^*|\bar{v}|^2 - \gamma^*\bar{u}\bar{v}\right]\cdot\sin^2\frac{\theta}{2}\cdot e^{-i\delta}. \end{aligned} \tag{58}$$

The three terms of Eq. (58) correspond, respectively, to the terms $T_1 + T_2 + T_3$ of Eq. (9).

For the first term, T_1, we use Eqs. (43), (41), and (40) to write

$$\beta^* = (n_x - in_y)\sin(N\ell) = \frac{1}{N}(f_0 + if_1)\sin(N\ell); \tag{59}$$

the term reduces immediately to

$$T_1 = (-i)s_{23}\frac{f}{N}\sin(\bar{N}\Delta)\cdot e^{-i\delta}. \tag{60}$$

Considering the second term T_2, we use Eqs. (47) and (51) to insert

$$\bar{u} = \frac{1}{\eta}(\gamma r + i\beta^*B)e^{iG\ell},\quad \bar{v}^* = \frac{1}{\eta}(\gamma^*B + i\beta r)e^{iG\ell},$$

and find that it reduces to

$$T_2 = (-i)c_{23}\frac{r}{\eta}\cdot\sin(\bar{\eta}\Delta)\cdot e^{i\bar{G}\Delta}. \tag{61}$$

The remaining term is

$$T_3 = 2s_{23}\left[i\beta^*|\bar{v}|^2 - \gamma^*\bar{u}\bar{v}\right]\cdot\sin^2\frac{\theta}{2}\cdot e^{-i\delta}. \tag{62}$$

The expression within the bracket reduces to $\frac{1}{\eta^2}\left[-\gamma rb + i\beta^*|r|^2\right]$ so that

$$T_3 = -2s_{23}\left\{\left(\frac{rb}{\eta^2}\right)\cdot\gamma - i\left(\frac{|r|^2}{\eta^2}\right)\cdot\beta^*\right\}. \tag{63}$$

Substitution of γ and β^* from Eq. (43) yields

$$T_3 = (-2s_{23})\cdot\sin^2\frac{\theta}{2}\cdot e^{-i\delta}\cdot \left\{\frac{rb}{\eta^2}\cos\phi + \left[\frac{-|r|^2 n_y}{\eta^2} + i\left(\frac{rb}{\eta^2}\cdot n_z - \frac{|r|^2}{\eta^2}n_x\right)\right]\sin\phi\right\}. \tag{64}$$

Within the curly brackets on the right-hand side, the factors multiplying $\cos\phi$ comprise the complex function S_1 of Eq. (23), and the expression which multiplies $\sin\theta$ is the complex function S_2 of Eq. (24). Thus Eq. (64) coincides with Eq. (25) for T_3.

With Eqs. (60), (61), and (64) we have shown that T_1, T_2, and T_3 have the forms as previously specified in Eqs. (18), (20), and (25) of Sec. III B. The transition amplitude $\mathcal{A}(\nu_\mu \to \nu_e)$ of Eq. (9) is thus completely specified.

[1] K. Abe *et al.* (T2K Collaboration), Phys. Rev. Lett. **107**, 041801 (2011).
[2] P. Adamson *et al.* (MINOS Collaboration), Phys. Rev. Lett. **107**, 181802 (2011).
[3] Y. Abe *et al.* (Double Chooz Collaboration), Phys. Rev. Lett. **108**, 131801 (2012).
[4] F.P. An *et al.* (Daya Bay Collaboration), Phys. Rev. Lett. **108**, 171803 (2012).
[5] J.K. Ahn *et al.* (RENO Collaboration), Phys. Rev. Lett. **108**, 191802 (2012).
[6] Y. Itow, plenary talk *in:* XXV Int. Conf. on Neutrino Physics and Astrophysics (NEUTRINO 2012), June 2012, Kyoto, Japan (to be published); (http://neu2012.kek.jp).
[7] P. Vahle *et al.* (MINOS Collaboration), Joint Experimental-Theoretical Seminar, Fermilab, 8 June 2012 (unpublished); (http://theory.fnal.gov/jetp/).
[8] Tommy Ohlsson, arXiv:1209.2710.
[9] L. Wolfenstein, Phys. Rev. D **17**, 2369 (1978); S. P. Mikheyev and A. Y. Smirnov, Yad. fiz. **42**, 1441 (1985) [Sov. J. Nucl. Phys. **42**, 913 (1985)]; S. P. Mikheyev and A. Y. Smirnov, Nuovo Cim. C **9**, 17 (1986).
[10] A. Friedland, M. L. Graesser, I. M. Shoemaker, and L. Vecchi, Phys. Lett. B **714**, 267 (2012); arXiv:1111.5331.
[11] H. Minakata, *In:* Proceedings of the 13th Int. Workshop on Neutrino Telescopes, Venice, Italy, March 2009, Milla Baldo Ceolin, Editor, p. 327; arXiv:0905.1387.
[12] H. Oki and O. Yasuda, Phys. Rev. D **82**, 073009 (2010); arXiv:1003.5554.
[13] J. Kopp, P.A.N. Machado, and S.J. Parke, Phys. Rev. D **82**, 113002 (2010); arXiv: 1009.0014.
[14] C. Biggio, M. Blennow, and E. Fernandez-Martinez, J. High En. Phys. **0908**, 090 (2009); arXiv:0907.0097.
[15] M.C. Gonzalez-Garcia, M. Maltoni, and J. Salvado, J. High En. Phys. **1105**, 075 (2011); arXiv:1103.4365.
[16] A. Bolanos, O.G. Miranda, A. Palazzo, M.A. Tortola, and J.W.F. Valle, Phys. Rev. D **79**, 113012 (2009); arXiv:0812.4417.
[17] A. Friedland and I.M. Shoemaker, arXiv:1207.6642.
[18] A. Friedland, C. Lunardini, and C. Peña-Garay, Phys. Lett. B **594**, 347 (2004).
[19] A. Palazzo and J.W.F. Valle, Phys. Rev. D **80**, 091301 (2009); arXiv:0909.1535.
[20] A. Palazzo, Phys. Rev. D **83**, 101701(R) (2011); arXiv:1101.3875.
[21] T. Nakaya *et al.* (T2K Collaboration), plenary talk, NEUTRINO 2012, June 2012 (to be published); (http://neu2012.kek.jp).
[22] R. Nichol *et al.* (MINOS Collaboration), plenary talk, NEUTRINO 2012, June 2012 (to be published); (http://neu2012.kek.jp).
[23] R. Adhikari, S. Chakraborty, A. Dasgupta, and S. Roy, arXiv:1201.3047.
[24] A. Friedland and C. Lunardini, Phys. Rev. D **74**, 033012 (2006).
[25] O. Yasuda, Acta Phys. Pol. B **38**, 3381 (2007).
[26] H. Sugiyama, AIP Conf. Proc. **981**, 216 (2008).
[27] M. Blennow, T. Ohlsson, and J. Skrotzki, Phys. Lett. B **660**, 522 (2008); arXiv:0804.2744.
[28] A. Esteban-Pretel, J.W.F. Valle, and P. Huber, Phys. Lett. B 668, 197 (2008).
[29] A. Friedland, C. Lunardini, and M. Maltoni, Phys. Rev. D **70**, 111301 (2004); arXiv:hep-ph/0408264.
[30] A. Friedland and C. Lunardini, Phys. Rev. D **72**, 053009 (2005); arXiv:hep-ph/0506143.
[31] W.A. Mann, T. Kafka, J. Schneps, and O. Altinok, arXiv:1204.6338.
[32] M. Blennow, D. Meloni, T. Ohlsson, F. Terranova and M. Westerberg, Eur. Phys. J. C **56**, 529 (2008); arXiv:0804.2744.
[33] N. Fornengo, M. Maltoni, R. Tomas Bayo, and J.W.F. Valle, Phys. Rev. D **65**, 013010 (2001); arXiv:hep-ph/0108043.
[34] M.C. Gonzalez-Garcia and M. Maltoni, Phys. Rev. D **70**, 033010 (2004); arXiv:hep-ph/0108043.
[35] A. Cervera, A. Donini, M.B. Gavela, J.J. Gomez Cadenas, P. Hernandez, O. Mena, and S. Rigolin, Nucl. Phys. B **579**, 17 (2000), Erratum-ibid, B **593**, 731 (2001); hep-

ph/0002108.
[36] M. Freund, Phys. Rev. D **64**, 053003 (2001); hep-ph/0103300.
[37] E. K. Akhmedov, R. Johansson, M. Lindner, T. Ohlsson, and T. Schwetz, J. High Energy Phys. 04 (2004) 078; hep-ph/0402175.
[38] G.L. Fogli, E. Lisi, A. Marrone, D. Montanino, A. Palazzo, and A.M. Rotunno, Phys. Rev. D **86**, 013012 (2012); arXiv:1205.5254.
[39] T. Ota, J. Sato, and N.a. Yamashita, Phys. Rev. D **65**, 093015 (2002).
[40] J. Kopp, M. Lindner, T. Ota, and J. Sato, Phys. Rev. D **77**, 013007 (2008).